J. Fluid Mech. (2006), *vol.* 549, *pp.* 375–384. © 2006 Cambridge University Press
doi:10.1017/S0022112005008189 Printed in the United Kingdom

On boundary-layer convection in a rotating fluid layer

By X. LIAO[1], K. ZHANG[2] AND Y. CHANG[1]

[1]Shanghai Astronomical Observatory, Chinese Academy of Sciences, Shanghai 200030, China
[2]Department of Mathematical Sciences, University of Exeter, Exeter EX4 4QE, UK

(Received 23 August 2005 and in revised form 16 November 2005)

The asymptotic solutions of second-order accuracy taking account of the velocity boundary conditions imposed on the sidewalls are derived for wall-localized boundary-layer convection in a rotating fluid layer in the presence of stress-free or no-slip vertical sidewalls. The second-order asymptotic solutions give a satisfactory quantitative agreement with the fully numerical solutions obtained in a rotating channel with either stress-free or no-slip sidewalls. Furthermore, we show, through fully three-dimensional numerical simulations, that the structure of the boundary-layer convection is highly robust in strongly nonlinear regimes.

1. Introduction

An intricate phenomenon in rotating planar systems is the occurrence of wall-localized boundary-layer convection when vertical sidewalls are present in the Bénard layer, such as a channel or a cylinder (see, for example, Davies-Jones & Gilman 1971; Zhong, Ecke & Steinberg 1991; Goldstein *et al.* 1993; Herrmann & Busse 1993; Kuo & Cross 1993; Liu & Ecke 1999; Plaut 2003; Liao, Zhang & Chang 2005). It has been demonstrated, both experimentally and theoretically, that the presence of no-slip vertical sidewalls in the Bénard layer destabilizes convection and causes overstability, resulting in boundary-layer convection when the systems rotate fast enough. It was also suggested that the effect of vanishing toroidal flow imposed on the no-slip sidewalls plays an important role in producing the boundary-layer phenomenon. In fact, all the previous studies of the problem assumed the no-slip velocity condition on the sidewalls. We do not understand fully why the phenomenon occurs in various rotating fluid systems. Demonstrating that boundary-layer convection also takes place in a rotating channel with stress-free sidewalls provides insight into the physical mechanism. Moreover, a higher-order asymptotic analysis taking account of the velocity boundary conditions imposed on the sidewalls, together with the corresponding numerical analysis, would help point to the nature of the phenomenon.

We first look at why an extremely small length scale is required for convective instabilities in a rapidly rotating unbounded Bénard layer of depth d. When the layer rotates rapidly, the fundamental dynamics of fluid motions can be intuitively illustrated by the Proudman–Taylor theorem (see, for example, Greenspan 1968) which states that infinitesimal steady motions in a rotating inviscid fluid (the Ekman number $E=0$, where $E=\nu/2\Omega d^2$, ν is kinematic viscosity and Ω is the angular velocity) are two-dimensional with respect to the direction of the angular rotation velocity. It follows that $\partial u_z/\partial z=0$, where u_z is the vertical component of the flow and z is the coordinate along the axis of rotation. Upon applying the velocity boundary condition

https://doi.org/10.1017/S0022112005008189 Published online by Cambridge University Press

on the lower and upper bounding surface of the Bénard layer, we must conclude that $u_z = 0$ uniformly within the fluid layer. In other words, convection cannot take place: the effect of rotation constrains and strongly stabilizes the system. The rotational constraint must be broken in order that convective instabilities can occur. Except for fluids of small Prandtl numbers (Zhang & Roberts 1997), the only way to break the rotational constraint is to invoke large viscosity in association with small-scale convection cells. It means that a small horizontal length scale, $O(dE^{1/3})$ as $E \to 0$, of convection is required to offset the constraint to allow convective instability. Because of the horizontal uniformity of the Bénard layer, the small-scale convection cells have to fill the unbounded layer uniformly at the onset of convective instabilities, although the precise planform of the flow cannot be determined as a result of the degeneracy of the linear problem.

The introduction of vertical sidewalls to the Bénard planar system, such as the geometries of a channel or a cylinder, destroys the horizontal uniformity of the layer. In this connection, it is helpful to compare uniformity in the Bénard layer to non-uniformity in spherical geometry. As a consequence of the variation of the angle between the gravity vector (normal vector of the spherical surface) and the rotation vector, convective motions in spherical geometry are usually highly localized, either in middle latitudes for large-Prandtl-number fluids (Busse 1970; Jones, Soward & Mussa 2000) or in the equatorial region for small-Prandtl-number fluids (Zhang 1994, 1995). The presence of sidewalls in the Bénard layer not only removes the horizontal uniformity but also creates particular regions in the vicinity of the sidewalls where travelling convective waves can be trapped. This yields an optimal condition for convective instability: the boundary-layer flow with thickness $O(dE^{1/3})$ maximizes the effect of viscous dissipation required to break the rotational constraint, while it also minimizes the vertical temperature gradient required to initiate convection via the spatial localization of the flow.

This paper undertakes both an asymptotic and numerical analysis of boundary-layer convection in a rotating fluid layer. Three new results are presented. First, we carry out a second-order asymptotic analysis for boundary-layer convection in a rotating fluid layer uniformly heated from below in the presence of lateral stress-free or no-slip sidewalls. The second-order asymptotic solutions are valid for a general planar fluid system with vertical sidewalls such as channels and cylinders. We reveal that it is necessary to obtain the higher-order terms in the asymptotic expansion in order to take account of the velocity condition imposed on the sidewalls. Second, we study boundary-layer convection in an annular channel rotating about a vertical axis with two sidewalls uniformly heated from below, first studied by Davies-Jones & Gilman (1971) and Gilman (1973). It is found numerically that the stress-free velocity condition on the sidewalls also gives rise to a similar planform of boundary-layer convection, suggesting that the no-slip velocity condition imposing vanishing toroidal component of the flow on the sidewalls plays an insignificant role in producing the boundary-layer phenomenon. A comparison between the fully numerical and second-order asymptotic solutions shows a satisfactory quantitative agreement. Third, we perform fully three-dimensional numerical simulations of the problem, finding that the structure of the boundary-layer convection is highly robust in strongly nonlinear regimes.

2. Numerical analysis

In the numerical analysis, we consider a Boussinesq fluid in an annular channel, heated from below, with constant thermal diffusivity κ, thermal expansion coefficient

https://doi.org/10.1017/S0022112005008189 Published online by Cambridge University Press

α and kinematic viscosity ν. The annular channel has depth d with vertical coordinate given by z, inward radial coordinate y and azimuthal coordinate x. Similar to previous studies, the effect of the annular curvature will be neglected. The aspect ratio, the width to depth of the channel, is denoted by Γ. The governing equations for the three-dimensional velocity $\boldsymbol{u}=(u_x, u_y, u_z)$ (with the unit vectors $(\boldsymbol{i}, \boldsymbol{j}, \boldsymbol{k})$), the pressure p and the temperature fluctuation Θ, are given by

$$\frac{\partial \boldsymbol{u}}{\partial t} + \boldsymbol{u}\cdot\nabla\boldsymbol{u} + \tau\boldsymbol{k}\times\boldsymbol{u} = -\nabla p + R\Theta\boldsymbol{k} + \nabla^2\boldsymbol{u}, \tag{2.1}$$

$$Pr\left(\frac{\partial \Theta}{\partial t} + \boldsymbol{u}\cdot\nabla\Theta\right) = \boldsymbol{u}\cdot\boldsymbol{k} + \nabla^2\Theta, \tag{2.2}$$

$$\nabla\cdot\boldsymbol{u} = 0. \tag{2.3}$$

The three non-dimensional parameters, the Rayleigh number R, the Prandtl number Pr and the rotation number τ, defined as

$$R = \frac{\alpha\beta g_0 d^4}{\nu\kappa}, \quad Pr = \frac{\nu}{\kappa}, \quad \tau = E^{-1} = \frac{2\Omega d^2}{\nu},$$

characterize the problem of convective instability. While the boundary conditions at the top ($z=1$) and bottom ($z=0$) are assumed to be stress-free and perfectly conducting, as in the previous studies (see, for example, Davies-Jones & Gilman 1971; Goldstein *et al.* 1993; Herrmann & Busse 1993; Busse 2005), on the sidewalls the present study assumes either stress-free, impenetrable and perfectly insulating conditions,

$$u_y = \frac{\partial u_x}{\partial y} = \frac{\partial u_z}{\partial y} = \frac{\partial \Theta}{\partial y} = 0 \qquad \text{at} \qquad y = 0, \Gamma, \tag{2.4}$$

or no-slip and perfectly insulating conditions

$$u_y = u_x = u_z = \frac{\partial \Theta}{\partial y} = 0 \qquad \text{at} \qquad y = 0, \Gamma. \tag{2.5}$$

We shall focus on the insulating condition since the primary features of the boundary-layer phenomenon are not affected by the temperature condition on the sidewalls (see, for example, Liao *et al.* 2005). We shall solve the convection problem both numerically and asymptotically, with the fully numerical solution providing an important comparison with and guidance to the asymptotic analysis.

In the first part of the numerical analysis, we consider the onset of convection, the linear version of equations (2.1)–(2.3), by expressing the velocity $\boldsymbol{u}$ as a sum of poloidal (Φ) and toroidal (Ψ) vectors,

$$\boldsymbol{u} = \nabla\times\nabla\times[\Phi(x, y, z, t)\boldsymbol{j}] + \nabla\times[\Psi(x, y, z, t)\boldsymbol{j}]. \tag{2.6}$$

In terms of Ψ and Φ, the boundary conditions on the stress-free sidewalls become

$$\Phi = \frac{\partial^2\Phi}{\partial y^2} = \frac{\partial \Psi}{\partial y} = \frac{\partial \Theta}{\partial y} = 0 \quad \text{at } y = 0, \Gamma, \tag{2.7}$$

while the conditions on the no-slip sidewalls are given by

$$\Phi = \frac{\partial \Phi}{\partial y} = \Psi = \frac{\partial \Theta}{\partial y} = 0 \quad \text{at } y = 0, \Gamma. \tag{2.8}$$

We anticipate that there exist two travelling wave solutions at a given Rayleigh number R: one propagates in the prograde direction (the positive x-direction) and

https://doi.org/10.1017/S0022112005008189 Published online by Cambridge University Press

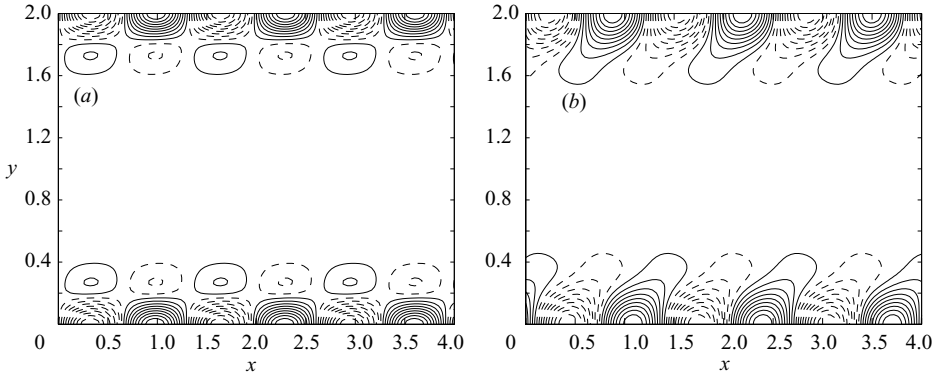

FIGURE 1. Contours of (*a*) u_z and (*b*) Θ of boundary-layer convection in the mid-plane (x, y-plane at $z=0.5$) of a channel with stress-free sidewall and $\Gamma=2$ for $\tau=10^3$, $Pr=7$ at the onset of convective instabilities with $R=R_c=2.55\times10^4$. Both the retrogradely and progradely travelling modes with $A_1=1$, $A_2=1$ are displayed.

the other in the retrograde direction (the negative x-direction) when τ is large enough and the aspect ratio $\Gamma \geqslant O(1)$. We then write numerical solutions at the onset of convection in the form

$$[\Psi, \Phi, \Theta] = \sum_{j=1}^{2} A_j [\Psi_j(y)\sin\pi z, \Phi_j(y)\cos\pi z, \Theta_j(y)\sin\pi z]\exp[\mathrm{i}ax + (-1)^j \omega t], \quad (2.9)$$

where $j=1$ or $j=2$, ω is assumed to be real and positive and a is the azimuthal wavenumber which is henceforth assumed to be positive $a>0$. This leads to three different solutions: (i) $A_1=1$ with $A_2=0$ (localized in the vicinity of the inner sidewall at $y=\Gamma$), (ii) $A_1=0$ with $A_2=1$ (localized in the vicinity of the outer sidewall at $y=0$) and (iii) $A_1=1$ and $A_2\neq0$ (localized in the vicinity of both the sidewalls, a linear superposition of independent modes (i) and (ii)). Our emphasis is on the planform of convective motions, in particular whether boundary-layer convection is still preferred in the absence of the no-slip velocity condition on the sidewall. For given a, Pr and τ, the linear version of (2.1)–(2.3) is solved numerically to determine the values of R and ω as well as complex coefficients in (2.9) for the marginal solution. Many similar computations are then repeated to determine the smallest Rayleigh number, R_c, the corresponding wavenumber a_c and frequency ω_c. In the second part of the numerical analysis, we perform fully three-dimensional numerical simulations for the governing equations (2.1)–(2.3) with various boundary conditions. Some preliminary results that are relevant to the boundary-layer convection are reported in this paper.

Three interesting features emerge from the numerical analysis. The first is that convection in rotating channels with stress-free sidewalls is also in the form of travelling waves and of boundary-layer flow, very similar to that in rotating channels with no-slip sidewalls. In consequence, the critical parameters are nearly independent of the aspect ratio Γ, as long as Γ is not too small, i.e. $\Gamma > O(\tau^{-1/3})$ (Busse 2005). The spatial structure of the boundary-layer convection (including both the prograde mode $\omega_c<0$ and the retrograde mode $\omega_c>0$) for $\tau=10^3$ with $Pr=7.0$ and $\Gamma=2$ is depicted in figure 1 at the onset of convection with $R=R_c=2.55\times10^4$. The second feature is that the structure of the linear boundary-layer convection is unexpectedly robust in strongly nonlinear regimes. Nonlinear convection solutions at $R=10^5$

https://doi.org/10.1017/S0022112005008189 Published online by Cambridge University Press

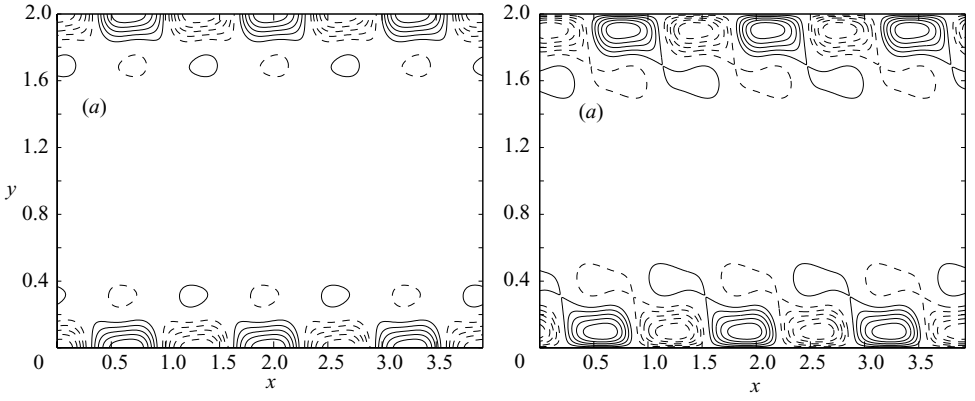

FIGURE 2. Contours of u_z obtained from three-dimensional numerical simulations in the mid-plane of a channel with (*a*) stress-free sidewalls and (*b*) no-slip sidewalls. The parameters for both the simulations are: $\Gamma = 2$, $\tau = 10^3$, $Pr = 7$ and $R = 10^5$.

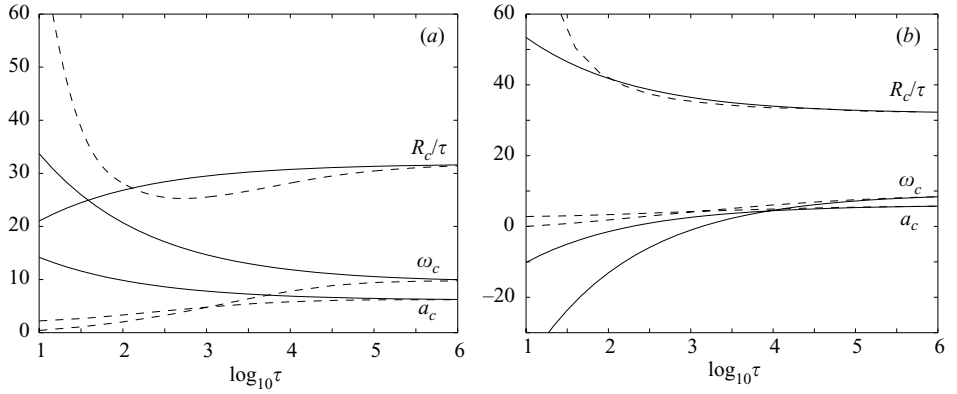

FIGURE 3. The critical parameters, a_c, R_c and ω_c, are plotted against the rotation parameter τ for $Pr = 7$: (*a*) shows the solutions with stress-free sidewalls and (*b*) no-slip sidewalls. Dashed lines represent the fully numerical solution in a channel with $\Gamma = 2$ while the solid lines denote the asymptotic solution.

(which are strongly nonlinear, $10^5 \approx 4R_c$) resulting from fully three-dimensional numerical simulations for both the stress-free and no-slip sidewalls are shown in figure 2, revealing nearly the same structure as for the linear solution although the amplitude of the nonlinear convection changes weakly periodically. The third feature is indicative of the existence of asymptotic dependence for large values of the rotation parameter τ for both the stress-free and no-slip sidewalls. In figure 3 (dashed lines), we show the dependence of the critical parameters, $R_c/\tau, a_c$ and ω_c, on τ in the range $10 \leqslant \tau \leqslant 10^6$. There are no significant variations in the critical parameters with increasing τ when $\tau \geqslant O(10^4)$. Our numerical solutions also show that the two critical parameters, R_c and a_c, are almost independent of Pr when τ is large enough, suggesting the asymptotic scalings for large τ: $R_c/\tau = O(1), \omega_c Pr = O(1), a_c = O(1)$, as $\tau \to \infty$, for boundary-layer convection with either stress-free or no-slip sidewalls, which will be adopted in our asymptotic analysis.

https://doi.org/10.1017/S0022112005008189 Published online by Cambridge University Press

3. Asymptotic analysis

In the asymptotic analysis, boundary condition (2.7) or (2.8) needs to be satisfied only at one sidewall, i.e. boundary-layer convection in the vicinity of that sidewall. Herrmann & Busse (1993) obtained the leading-order asymptotic solution for large rotation parameter τ for boundary-layer convection with a no-slip sidewall. However, we shall show that it is necessary to obtain the higher-order terms in the asymptotic expansion in order to take account of the velocity boundary condition imposed on the sidewalls.

We anticipate that the radial scale of the boundary-layer convection is $O(E^{1/3})$ or $O(\tau^{-1/3})$ in the cases of either stress-free or no-slip sidewalls, which is required to break the rotational constraint at the onset of convective instabilities. For sufficiently large values of τ, we therefore express solutions of the boundary-layer convection in the form

$$[\Psi, \Phi, \Theta] = [\tilde{\Psi} \sin \pi z, \tilde{\Phi} \cos \pi z, \tilde{\Theta} \sin \pi z] \exp[-\mu \hat{y}/\delta + \mathrm{i}(ax + (-1)^j \omega t)], \tag{3.1}$$

where $\mathrm{Re}\,[\mu] > 0$ and $\delta = E^{1/3} \ll 1$. For a channel, we take $j = 1$ with $\hat{y} = (\Gamma - y)$ or $j = 2$ with $\hat{y} = y$. The asymptotic analyses for $j = 1$ and 2 are nearly identical so we will only discuss the case $j = 2$. For a cylinder, there exists only one solution with $j = 2$ and $\hat{y} = (s_0 - s)$ while a is replaced by the azimuthal wavenumber $m = as_0$, where s_0 denotes the radius of the cylinder and s is the distance from the axis of rotation.

Substitution of (3.1) into the equations for Ψ, Φ, and Θ and elimination of the constant coefficients such as $\tilde{\Psi}$ and $\tilde{\Phi}$ yields an equation for μ as a function of other parameters of the problem

$$\begin{aligned} 0 = {} & [\mathrm{i}\pi^2(Pr + \tilde{R}\delta^2)\tilde{\omega} + \hat{a}^2(\pi^2 - \mathrm{i}\tilde{\omega}\tilde{R})\delta^2 + O(\delta^4)] \\ & + [-\pi^2(1 + \tilde{R}\delta^2) + 2\hat{a}^2(\tilde{R} + \tilde{\omega}^2 + 2Pr\tilde{\omega}^2)\delta^2 + \mathrm{i}\tilde{\omega}(\tilde{R} + Pr\delta^2\tilde{\omega}) + O(\delta^4)]\mu^2 \\ & + [-\tilde{R} - (1 + 2Pr)\tilde{\omega}^2 + 3\mathrm{i}\hat{a}^2(2 + Pr)\tilde{\omega}\delta^2 + O(\delta^4)]\mu^4 \\ & + [-4\hat{a}^2\delta^2 - \mathrm{i}(2 + Pr)\tilde{\omega}]\mu^6 + \mu^8, \end{aligned} \tag{3.2}$$

where $\hat{a}^2 = a^2 + \pi^2$, $\tilde{R} = \delta^4 R$, $\tilde{\omega} = \delta^2 \omega$. Generally, there exist eight complex roots for (3.2) of which the four roots with positive real part are relevant to the asymptotic solutions of the boundary-layer convection. Once the four roots, μ_j, $j = 1, 2, 3, 4$, are found, the asymptotic solution of the boundary-layer convection can be simply written as

$$\left.\begin{aligned} \Theta &= \sum_{j=1}^{4} -(\pi\hat{a}^2)\left[\mu_j\left(\mu_j^2 - \delta^2\hat{a}^2 - \mathrm{i}\tilde{\omega}\right) + \mathrm{i}a\right] X_j \sin \pi z \mathrm{e}^{-\mu_j \hat{y}/\delta + \mathrm{i}(ax + \omega t)}, \\ \Phi &= \sum_{j=1}^{4} \frac{1}{\delta}\left[\hat{a}^2\left(\mu_j^2 - \delta^2\hat{a}^2 - \mathrm{i}\tilde{\omega}\right)\left(\mu_j^2 - \delta^2\hat{a}^2 - \mathrm{i}Pr\tilde{\omega}\right) - \tilde{R}a^2\right] \\ &\quad \times X_j \cos \pi z \mathrm{e}^{-\mu_j \hat{y}/\delta + \mathrm{i}(ax + \omega t)}, \\ \Psi &= \sum_{j=1}^{4} \frac{\pi}{\delta^2}\left[\hat{a}^2\left(\mu_j^2 - \delta^2\hat{a}^2 - \mathrm{i}Pr\tilde{\omega}\right) - \mathrm{i}\mu_j\tilde{R}a\right] X_j \sin \pi z \, \mathrm{e}^{-\mu_j \hat{y}/\delta + \mathrm{i}(ax + \omega t)}, \end{aligned}\right\} \tag{3.3}$$

where the critical parameters and X_j can be determined by the four boundary conditions at $\hat{y} = 0$, which imposes the solvability condition of the linear system.

The mathematical problem can be solved in two stages. First, we must find the four roots with real positive part, μ_j, $j = 1, 2, 3, 4$. For an asymptotically small δ, we

https://doi.org/10.1017/S0022112005008189 Published online by Cambridge University Press

make use of the expansions in terms of δ,

$$\left.\begin{aligned} &\tilde{R} = \tilde{R}_1\delta + \tilde{R}_2\delta^2 + \ldots, \\ &\mu_j = (\mu_0)_j + (\mu_1)_j\delta + (\mu_2)_j\delta^2 + \ldots, \quad j = 1, 2, 3, 4, \\ &\tilde{\omega} = \tilde{\omega}_1\delta + \tilde{\omega}_2\delta^2 + \tilde{\omega}_3\delta^3 \ldots. \end{aligned}\right\} \tag{3.4}$$

Upon inserting the expansions (3.4) into equation (3.2), we solve the resulting equation, cumbersome but straightforward, for $(\mu_k)_j$, $j = 1, 2, 3, 4$ up to the second order δ^2 for $k = 0, 1, 2$. The leading-order equation gives

$$\left.\begin{aligned} &(\mu_0)_1 = 0, (\mu_0)_2 = \pi^{1/3}, \\ &(\mu_0)_3 = \tfrac{1}{2}\pi^{1/3}(1 + \mathrm{i}\sqrt{3}), (\mu_1)_4 = \tfrac{1}{2}\pi^{1/3}(1 - \mathrm{i}\sqrt{3}). \end{aligned}\right\} \tag{3.5}$$

The $O(\delta)$ equation leads to $\tilde{\omega}_1 = 0$ as well as

$$(\mu_1)_1 = (\hat{a}^2 + \mathrm{i}Pr\tilde{\omega}_2)^{1/2}, \quad (\mu_1)_2 = \frac{\tilde{R}_1}{6\pi}, \qquad (\mu_1)_3 = -\frac{\tilde{R}_1}{6\pi}, \quad (\mu_1)_4 = -\frac{\tilde{R}_1}{6\pi}. \tag{3.6}$$

For the $O(\delta)^2$ problem, we obtain

$$\left.\begin{aligned} (\mu_2)_1 &= \frac{\mathrm{i}Pr\tilde{\omega}_3(\hat{a}^2 - \mathrm{i}Pr\tilde{\omega}_2)^{1/2}}{2\sqrt{\hat{a}^4 + (Pr\tilde{\omega}_2)^2}}, \\ (\mu_2)_2 &= \frac{\hat{a}^2}{2\pi^{1/3}} - \frac{\tilde{R}_1^2}{72\pi^{7/3}} + \frac{\tilde{R}_2}{6\pi} + \left[\frac{\tilde{\omega}_2}{3\pi^{1/3}}\right]\mathrm{i}, \\ (\mu_2)_3 &= \frac{\hat{a}^2}{4\pi^{1/3}} - \frac{\tilde{R}_1^2}{144\pi^{7/3}} - \frac{\tilde{R}_2}{6\pi} + \frac{\sqrt{3}\tilde{\omega}_2}{6\pi^{1/3}} + \frac{1}{\pi^{1/3}}\left[\frac{\tilde{\omega}_2}{6} - \frac{\sqrt{3}\hat{a}^2}{4} + \frac{\sqrt{3}R_1^2}{144\pi^2}\right]\mathrm{i}, \\ (\mu_2)_4 &= \frac{\hat{a}^2}{4\pi^{1/3}} - \frac{\tilde{R}_1^2}{144\pi^{7/3}} - \frac{\tilde{R}_2}{6\pi} - \frac{\sqrt{3}\tilde{\omega}_2}{6\pi^{1/3}} + \frac{1}{\pi^{1/3}}\left[\frac{\tilde{\omega}_2}{6} + \frac{\sqrt{3}\hat{a}^2}{4} - \frac{\sqrt{3}R_1^2}{144\pi^2}\right]\mathrm{i}. \end{aligned}\right\} \tag{3.7}$$

For a stress-free sidewall, the solvability condition of the system is derived by demanding that the four boundary conditions (2.7) are satisfied at $\hat{y} = 0$, which yields

$$\det\{|M_{4\times4}|\} = 0, \tag{3.8}$$

where the elements of M_{kj} are

$$\left.\begin{aligned} M_{1j} &= \hat{a}^2\left(\mu_j^2 - \delta^2\hat{a}^2 - \mathrm{i}\tilde{\omega}\right)\left(\mu_j^2 - \delta^2\hat{a}^2 - \mathrm{i}Pr\tilde{\omega}\right) - \tilde{R}a^2, \quad j = 1, 2, 3, 4; \\ M_{2j} &= \mu_j^2\left[\hat{a}^2\left(\mu_j^2 - \delta^2\hat{a}^2 - \mathrm{i}\tilde{\omega}\right)\left(\mu_j^2 - \delta^2\hat{a}^2 - \mathrm{i}Pr\tilde{\omega}\right) - \tilde{R}a^2\right], \quad j = 1, 2, 3, 4; \\ M_{3j} &= \mu_j\left[\hat{a}^2\left(\mu_j^2 - \delta^2\hat{a}^2 - \mathrm{i}Pr\tilde{\omega}\right) - \mathrm{i}a\mu_j\tilde{R}\right], \quad j = 1, 2, 3, 4; \\ M_{4j} &= \mu_j\left[\mu_j\left(\mu_j^2 - \delta^2\hat{a}^2 - \mathrm{i}\tilde{\omega}\right) + \mathrm{i}a\right], \quad j = 1, 2, 3, 4. \end{aligned}\right\} \tag{3.9}$$

After inserting the expansions (3.4) into (3.8) and using (3.5)–(3.7), we then expand the resulting equation in terms of δ. Real and imaginary parts of the $O(\delta)$ term are used to determine the Rayleigh number $\tilde{R}_1$ and the frequency $\tilde{\omega}_2$, which are

$$\tilde{R}_1 = \left[\frac{\pi^2\hat{a}^2(a^2 - \pi^2)}{a^2} + \frac{4\pi^4\hat{a}^2}{(a^2 - \pi^2)}\right]^{1/2}, \qquad \tilde{\omega}_2 = \frac{2a\pi\hat{a}^2}{Pr(a^2 - \pi^2)}. \tag{3.10}$$

In the case of a no-slip sidewall, the solvability condition of the system is derived by demanding (2.8) be satisfied at $\hat{y} = 0$. In this case, the elements of M_{kj} are given

https://doi.org/10.1017/S0022112005008189 Published online by Cambridge University Press

by

$$\left.\begin{aligned}
&M_{1j} = \hat{a}^2\left(\mu_j^2 - \delta^2\hat{a}^2 - \mathrm{i}\tilde{\omega}\right)\left(\mu_j^2 - \delta^2\hat{a}^2 - \mathrm{i}Pr\tilde{\omega}\right) - \tilde{R}a^2, \quad j = 1, 2, 3, 4;\\
&M_{2j} = \mu_j\left[\hat{a}^2\left(\mu_j^2 - \delta^2\hat{a}^2 - \mathrm{i}\tilde{\omega}\right)\left(\mu_j^2 - \delta^2\hat{a}^2 - \mathrm{i}Pr\tilde{\omega}\right) - \tilde{R}a^2\right], \quad j = 1, 2, 3, 4;\\
&M_{3j} = \left[\hat{a}^2\left(\mu_j^2 - \delta^2\hat{a}^2 - \mathrm{i}Pr\tilde{\omega}\right) - \mathrm{i}a\mu_j\tilde{R}\right], \quad j = 1, 2, 3, 4;\\
&M_{4j} = \mu_j\left[\mu_j\left(\mu_j^2 - \delta^2\hat{a}^2 - \mathrm{i}\tilde{\omega}\right) + \mathrm{i}a\right], \; j = 1, 2, 3, 4.
\end{aligned}\right\} \tag{3.11}$$

By the same procedure, we are able to show that the velocity boundary condition does not enter the $O(\delta)$ problem in the solvability condition. In other words, the stress-free sidewall gives rise to the same $\tilde{R}_1$ and $\tilde{\omega}_2$ as the no-slip sidewall at the leading-order approximation. We expect that the effect of the velocity boundary condition enters the asymptotic solution in the $O(\delta^2)$ problem. This is again similar to the asymptotic convection solution in a rapidly rotating sphere in which only vanishing radial flow on the spherical container is required in the leading-order asymptotic analysis (see e.g. Busse 1970; Jones *et el.* 2000).

To reveal the effect resulting from the velocity boundary condition on the sidewalls, we must solve the higher-order problems to determine the second non-zero terms in the asymptotic expansion (3.4), i.e. to find $\tilde{R}_2$ and $\tilde{\omega}_3$ as a function of a and other parameters. We shall not write out the analytical expression explicitly because it is too lengthy. After obtaining the expression for $\tilde{R}_2$, it is then necessary to determine the critical wavenumber a_c of a that minimizes $(\tilde{R}_1 + \tilde{R}_2\delta)$, which gives rise to

$$a_c = (2+\sqrt{3})^{1/2}\pi + 17.49\tau^{-1/3}. \tag{3.12}$$

Substitution of a_c into the expressions for the Rayleigh number and frequency yields the asymptotic dependence of the critical Rayleigh number R_c and the frequency ω_c on τ in the case of the stress-free sidewall

$$R_c = \pi^2\left[\frac{6(9+5\sqrt{3})}{5+3\sqrt{3}}\right]^{1/2}\tau - 23.25\tau^{2/3}, \tag{3.13}$$

$$\omega_c = \left[\frac{2\pi^2(2+\sqrt{3})^{1/2}(3+\sqrt{3})}{(1+\sqrt{3})Pr} + 366.1\frac{\tau^{-1/3}}{Pr}\right](-1)^j, \quad j = 1, 2. \tag{3.14}$$

The asymptotic solution in the case of the stress-free sidewall is shown in figure 3(*a*), together with the fully numerical solutions for $Pr = 7.0$ in a channel with $\Gamma = 2$. It should be noted the second-order asymptotic formulas (3.12)–(3.14) are valid for general planar systems with the presence of vertical sidewalls such as cylinders and channels because of the nature of the boundary-layer phenomenon.

With a similar analysis, we also obtain the asymptotic expressions for the critical wavenumber a_c, the critical Rayleigh number R_c and the frequency ω_c for large values of τ in the case of the no-slip sidewalls

$$a_c = (2+\sqrt{3})^{1/2}\pi - 34.97\tau^{-1/3}, \tag{3.15}$$

$$R_c = \pi^2\left[\frac{6(9+5\sqrt{3})}{5+3\sqrt{3}}\right]^{1/2}\tau + 46.49\tau^{2/3}, \tag{3.16}$$

$$\omega_c = \left[\frac{2\pi^2(2+\sqrt{3})^{1/2}(3+\sqrt{3})}{(1+\sqrt{3})Pr} - 732.2\frac{\tau^{-1/3}}{Pr}\right](-1)^j, \; j = 1, 2. \tag{3.17}$$

The asymptotic solution for the no-slip sidewall is shown in figure 3(*b*) together with the corresponding fully numerical solutions for $Pr = 7.0$ and $\Gamma = 2$. Note that the

https://doi.org/10.1017/S0022112005008189 Published online by Cambridge University Press

presence of the no-slip condition at the top and bottom, which produces the vertical flux from the Ekman boundary layers, does not alter the asymptotic expressions. This is because boundary-layer convection only takes place in the narrow region (figure 1) with thickness $O(\tau^{-1/3})$, which together with the Ekman boundary-layer flux $O(\tau^{-1/2})$ would give rise to higher-order contributions in the asymptotic expansions (3.12)–(3.14) or (3.15)–(3.17).

Note that the sign of all the second non-zero terms in the asymptotic expansions (3.12)–(3.14), which represent the effect of the velocity boundary condition, is opposite to that in (3.15)–(3.17). This implies that convective instabilities in a stress-free-sidewall system occur much more easily than in a system with no-slip sidewalls. As a result of the significant higher-order terms in the expansion, the asymptotic solution approaches the corresponding fully numerical solution for moderate values $\tau \geqslant O(10^4)$.

For the purpose of comparison, we also derived the asymptotic expression of second-order accuracy for an unbounded Bénard layer, at moderate or large Pr, by removing the sidewalls (i.e. periodic boundary conditions in the y-direction),

$$a_c = \left(\tfrac{1}{2}\pi^2\right)^{1/6}\tau^{1/3} - \tfrac{1}{2}\left(\tfrac{1}{2}\pi^2\right)^{5/6}\tau^{-1/3}, \tag{3.18}$$

$$R_c = 3\left(\tfrac{1}{2}\pi^2\right)^{2/3}\tau^{4/3} + 3\left(\tfrac{1}{2}\pi^8\right)^{1/3}\tau^{2/3}, \tag{3.19}$$

$$\omega_c = 0. \tag{3.20}$$

At first glance, the critical wavenumbers in rapidly rotating channels and unbounded layers are fundamentally different. It should be noted however, that, while a_c in (3.12) or (3.15) represents the azimuthal wavenumber, a_c in (3.18) denotes the total wavenumber of convection cells. In terms of the smallest length scale of convection, they are the same of $O(\tau^{-1/3})$ as $\tau \to \infty$. Another important similarity between the asymptotic expressions (3.12)–(3.14) or (3.15)–(3.17) and (3.18)–(3.20) is their independence of the Prandtl number Pr (in the case of ω_c after an appropriate scaling by Pr).

4. Summary and remarks

We have derived the first asymptotic solutions of second-order accuracy that take account of the velocity boundary conditions imposed on the sidewalls for boundary-layer convection. The higher-order corrections due to the velocity condition on the sidewall lead to a quantitative agreement between the fully numerical and asymptotic solutions for moderately large τ, shown in figure 3, for both the stress-free and no-slip sidewalls. Our fully three-dimensional numerical simulations of the problem show that the basic structure of the boundary-layer convection remains nearly unchanged in strongly nonlinear regimes. The second-order asymptotic expressions given by (3.15)–(3.17) (or (3.12)–(3.14)) are particularly useful because they are not only independent of geometries but also valid for experimental boundary conditions.

By revealing that boundary-layer convection is also preferred in a channel with stress-free sidewalls, we shed valuable light on the understanding of this intriguing phenomenon. It is profitable to compare the boundary layer shown in figure 1 with the usual Ekman boundary layer (Greenspan 1968), both of which are caused by the effect of rapid rotation. The thickness of the Ekman boundary layer is mainly determined by the type of velocity condition on the sidewall. In contrast, the thickness of the wall-localized convection layer is not affected by the type of velocity boundary condition

https://doi.org/10.1017/S0022112005008189 Published online by Cambridge University Press

on the wall. It is determined by the interplay between the rotational constraint and how the convective motions break it. Without the presence of a sidewall in the Bénard layer, the constraint must be broken by the convective motions, with the concomitant length scale $\tau^{-1/3}$, everywhere as $\tau \to \infty$. The presence of a stress-free sidewall, requiring the vanishing of the normal flow on the sidewall, destroys the horizontal uniformity of planar geometry. It also creates a unique location where a wall-localized travelling wave with the required short scale $\tau^{-1/3}$ can be trapped. Because the short-scale convection occurs primarily in the thin boundary layer, instead of the whole horizontal layer, the rate of viscous dissipation and hence the critical Rayleigh number R_c are dramatically reduced, leading to a highly robust form of boundary-layer convection in a rotating fluid layer.

X. L. is supported by NSFC grant/10133010. K. Z., supported by PPARC, NERC and Leverhulme grants, would like to thank F. H. Busse for helpful discussions. The numerical computation was supported by the Shanghai Supercomputer Centre.

REFERENCES

Busse, F. H. 1970 Thermal instabilities in rapidly rotating systems. *J. Fluid Mech.* **44**, 441–460.

Busse, F. H. 2005 Convection in a narrow annular channel rotating about its axis of symmetry. *J. Fluid Mech.* **537**, 145–154.

Davies-Jones, R. P. & Gilman, P. A. 1971 Convection in a rotating annulus uniformly heated from below. *J. Fluid Mech.* **46**, 65–81.

Gilman, P. A. 1973 Convection in a rotating annulus uniformly heated from below. Part 2. Nonlinear results. *J. Fluid Mech.* **57**, 381–400.

Goldstein, H. F., Knobloch, E., Mercader, I. & Net, M. 1993 Convection in a rotating cylinder. Part 1. Linear theory for moderate Prandtl numbers. *J. Fluid Mech.* **248**, 583–604.

Greenspan, H. P. 1968 *The Theory of Rotating Fluids*. Cambridge University Press.

Herrmann, J. & Busse, F. H. 1993 Asymptotic theory of wall-localized convection in a rotating fluid layer. *J. Fluid Mech.* **255**, 183–194.

Jones, C. A., Soward, A. M. & Mussa, A. I. 2000 The onset of thermal convection in a rapidly rotating sphere. *J. Fluid Mech.* **405**, 157–179.

Kuo, E. Y. & Cross, M. C. 1993 Travelling-wall wall states in rotating Rayleigh-Benard convection. *Phys. Rev.* E **47**, 2245–2248.

Liao, X., Zhang, K. & Chang, Y. 2005 Convection in rotating annular channels heated from below: Part 1. Linear stability and weakly nonlinear mean flows. *Geophys. Astrophys. Fluid Dyn.* **99**, 445–465.

Liu, Y. & Ecke, R. E. 1999 Nonlinear traveling waves in rotating Rayleigh-Bnard convection: Stability boundaries and phase diffusion. *Phys. Rev.* E **59**, 4091–4105.

Plaut, E. 2003 Nonlinear dynamics of travelling Rayleigh-Bénard convection: effects of the boundary conditions and of the topology. *Phys. Rev.* E **67**, 046303.

Zhang, K. 1994 On coupling between the Poincaré equation and the heat equation. *J. Fluid Mech.* **268**, 211–229.

Zhang, K. 1995 On coupling between the Poincaré equation and the heat equation: non-slip boundary condition. *J. Fluid Mech.* **284**, 239–256.

Zhang, K. & Roberts P. H. 1997 Thermal inertial waves in a rotating fluid layer: exact and asymptotic Solutions. *Phys. Fluids* **9**, 1980–1987.

Zhong, F., Ecke, R. E. & Steinberg, V. 1991 Asymmetric modes and the transition to vortex structure in rotating Rayleigh-Benard convection. *Phys. Rev. Lett.* **67**, 2473–2476.

https://doi.org/10.1017/S0022112005008189 Published online by Cambridge University Press